Novel mechanisms of eIF2B action and regulation by eIF2α phosphorylation

Andrew M. Bogorad, Kai Ying Lin & Assen Marintchev

Boston University School of Medicine, Dept. of Physiology & Biophysics, Boston, MA, 02118

Supplementary Material

Supplementary Methods, one Supplementary Table, nine Supplementary Figures, and Supplementary References.

Table S1. Docking eIF2α on eIF2B

Docking model	Binding partner	Distances				
		NMR[1]			Cross-link[2]	
		< 5 Å (%)	< 10 Å (%)	> 10 Å (%)	< 10 Å (%)	< 15 Å (%)
NMR + cross-linking (this work)	eIF2Bα	14 67 %	21 100 %	0 0 %	7 88 %	8 100 %
	eIF2Bβ	6 38 %	11 69 %	5 31 %	4 67 %	6 100 %
	eIF2Bδ				3 100 %	3 100 %
Cross-linking only (1)[3]	eIF2Bα	7 33 %	14 67 %	7 33 %	7 88 %	8 100 %
	eIF2Bβ	3 19 %	7 44 %	9 56 %	6 100 %	6 100 %
	eIF2Bδ				3 100 %	3 100 %

[1] NMR distance restraints were set to 5 Å. Distances < 10 Å were considered allowed, to account for docking the proteins as rigid bodies, and docking human eIF2α to *S. pombe* eIF2B. Distances > 10 Å were considered restraint violations.

[2] Cross-linking distance restraints were set to 10 Å. Distances < 15 Å were considered allowed, to account for docking the proteins as rigid bodies, and docking human eIF2α to *S. pombe* eIF2B. Distances > 15 Å were considered restraint violations (no such restraint violations were observed in any of the two docking models).

[3] Analyzed as a reference.

Fig. S1

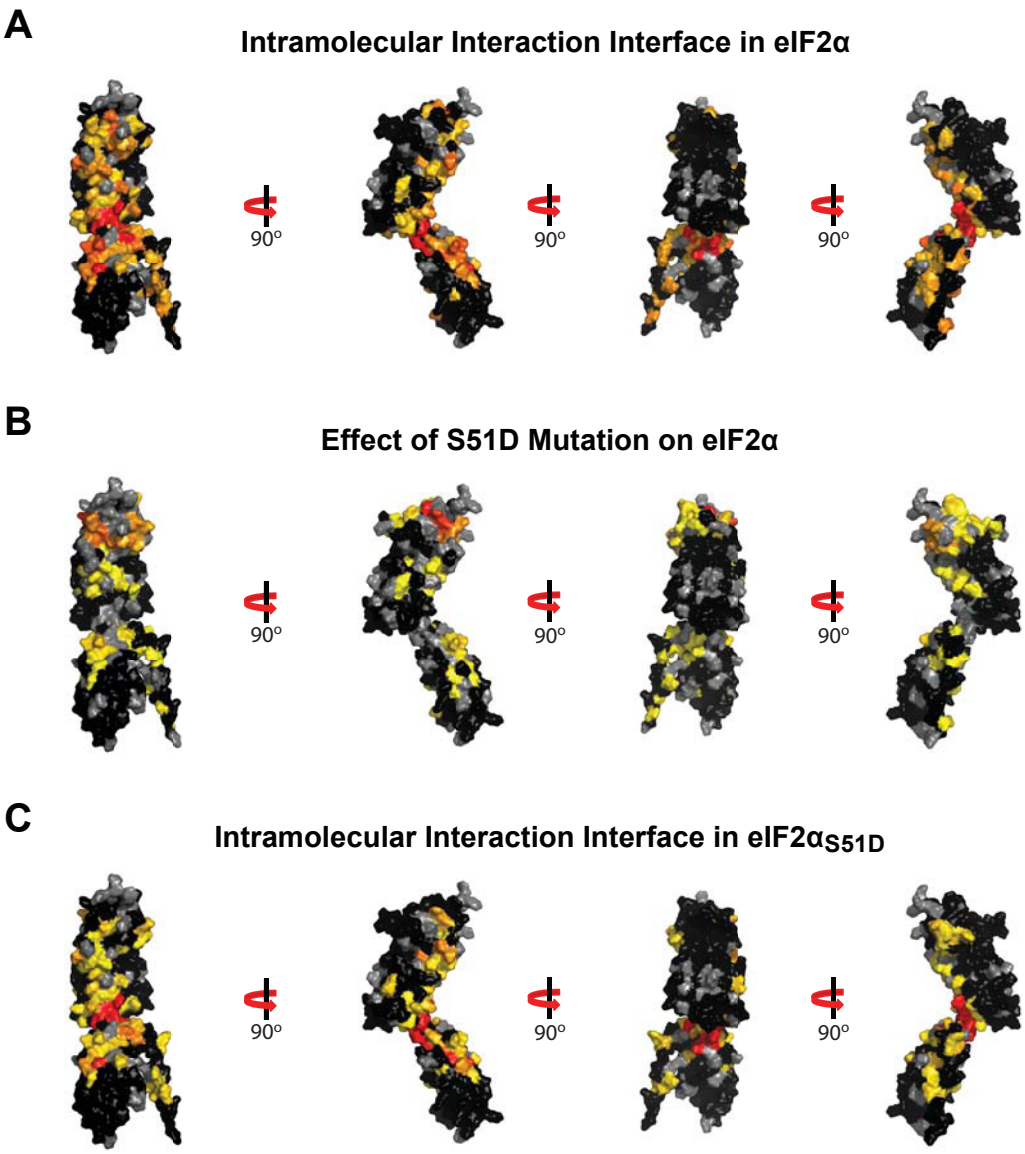
A
Intramolecular Interaction Interface in eIF2α
90°
90°
90°
B
Effect of S51D Mutation on eIF2α
90°
90°
90°
C
Intramolecular Interaction Interface in eIF2α$_{S51D}$
90°
90°
90°

Figure S1. Comparisons of the CSP effects of the phosphomimetic mutation S51D and deletion analysis of the eIF2α intermolecular interaction

(A) Residues affected by the intramolecular interaction mapped onto the structure of eIF2α, colored from **yellow** (>1 standard deviation (σ)) to **red** (>3σ). Indeterminate residues are colored **grey**. Residues <1σ are colored **black**. A contiguous surface is apparent, also involving the CTT. Residues 302-314 were absent in the NMR structure and are thus not displayed here and were not obviously affected. This panel is identical to **Fig. 1D**. **(B)** Residues affected by the phosphomimetic mutation mapped onto the structure of eIF2α. Coloring is as in panel *A*. Comparison to panel *A* reveals that the effects of the phosphomimetic mutation overlap substantially with the intramolecular surface, but are of smaller magnitude. This panel is identical to **Fig. 2D**. **(C)** Residues affected by the intramolecular interaction in eIF2α_{S51D} mapped onto the structure of eIF2α, colored as in panel *A*. Comparison to panel *A* reveals that the effects of the intramolecular interaction in eIF2α_{S51D} are essentially the same as in WT eIF2α, but are of smaller magnitude.

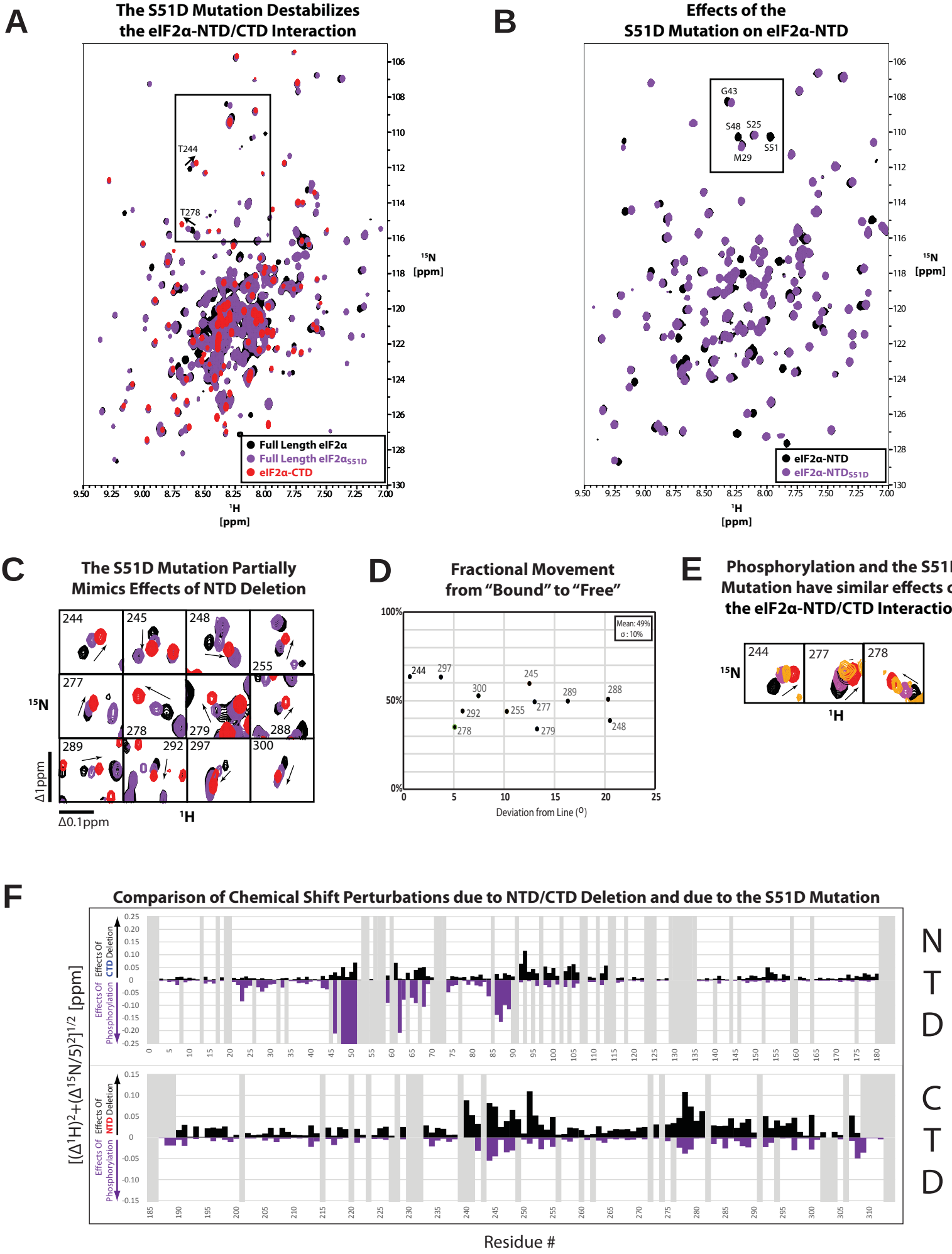
A
The S51D Mutation Destabilizes the eIF2α-NTD/CTD Interaction
T244
T278
Full Length eIF2α
Full Length eIF2α$_{S51D}$
eIF2α-CTD
^{15}N [ppm]
^{1}H [ppm]
B
Effects of the S51D Mutation on eIF2α-NTD
G43
S48
S25
S51
M29
eIF2α-NTD
eIF2α-NTD$_{S51D}$
^{15}N [ppm]
^{1}H [ppm]
C
The S51D Mutation Partially Mimics Effects of NTD Deletion
244
245
248
255
277
278
279
288
289
292
297
300
^{15}N
Δ1ppm
Δ0.1ppm
^{1}H
D
Fractional Movement from "Bound" to "Free"
Mean: 49%
σ : 10%
100%
50%
0%
244
297
300
245
289
288
292
255
277
278
279
248
0
5
10
15
20
25
Deviation from Line (°)
E
Phosphorylation and the S51D Mutation have similar effects on the eIF2α-NTD/CTD Interaction
244
277
278
^{15}N
^{1}H
F
Comparison of Chemical Shift Perturbations due to NTD/CTD Deletion and due to the S51D Mutation
Effects Of CTD Deletion
Effects Of Phosphorylation
Effects Of NTD Deletion
Effects Of Phosphorylation
$[(\Delta^1H)^2+(\Delta^{15}N/5)^2]^{1/2}$ [ppm]
NTD
CTD
Residue #

Figure S2. Effects of the phosphomimetic mutation S51D on the eIF2α intermolecular interaction

(A) TROSY-HSQC spectra of $^{2}H/^{15}N$-labeled full length eIF2α (**black**), full length phosphomimetic eIF2α (**purple**), and $^{2}H/^{15}N/^{13}C$-labeled eIF2α-CTD (**red**). Arrows indicate movement of peaks away from their full length WT positions. The boxed area corresponds to the blown up frame shown in Figure 2E. **(B)** TROSY-HSQC spectra of $^{2}H/^{15}N$-labeled eIF2α-NTD (**black**) and phosphomimetic eIF2α-NTD_{S51D} (**purple**). **(C)** Shown in individual insets are peaks for eIF2α-CTD residues experiencing chemical shift perturbations of 1σ or greater, derived from the spectra comparison shown in *(A)*. The pattern of peak movement indicates a destabilizing effect of the phosphomimetic mutation on the intramolecular interaction in eIF2α, since the peaks in the phosphomimetic eIF2α mutant are intermediate between the peak positions in full-length WT eIF2α and those in free eIF2α-CTD. **(D)** For the residues highlighted in *(C)*, the fractional displacement along the line and the magnitude of deviation off of the line were calculated. A value of 100% corresponds to final location on top of the eIF2α-CTD peak position, while a value of 0% indicates no movement and thus a final location on top of the wild-type eIF2α peak position. Resulting mean fractional displacement of ~50% indicates peak positions are halfway between eIF2α ("bound" state) and eIF2α-CTD ("free" state). No pattern emerged based on angular deviation. **(E)** Shown in individual insets are select peaks for eIF2α-CTD residues from *(C)*, with the peak from the spectrum of phosphorylated full-length eIF2α overlaid in gold over the spectra of full-length eIF2α (**black**), full length phosphomimetic eIF2α (**purple**), and eIF2α-CTD (**red**). The pattern of peak movement indicates a slightly greater destabilizing effect on the intramolecular interaction in eIF2α by phosphorylation, compared to the phosphomimetic mutation, since the peaks in phosphorylated eIF2α are slightly closer to the peak position in free eIF2α-CTD. **(F)** Plot of chemical shift perturbations due to deletion of the opposite domain (**black**) as well as due to the phosphomimetic mutation (**purple**). **Grey** bars represent indeterminate residues for which no analysis could be performed. A substantial overlap exists between residues affected by intramolecular interaction and by the S51D mutation, as can also be visually seen by comparing **Fig. S1A** and **B**.

Fig. S3

A **Closed eIF2α conformation in the context of the eIF2 structure**

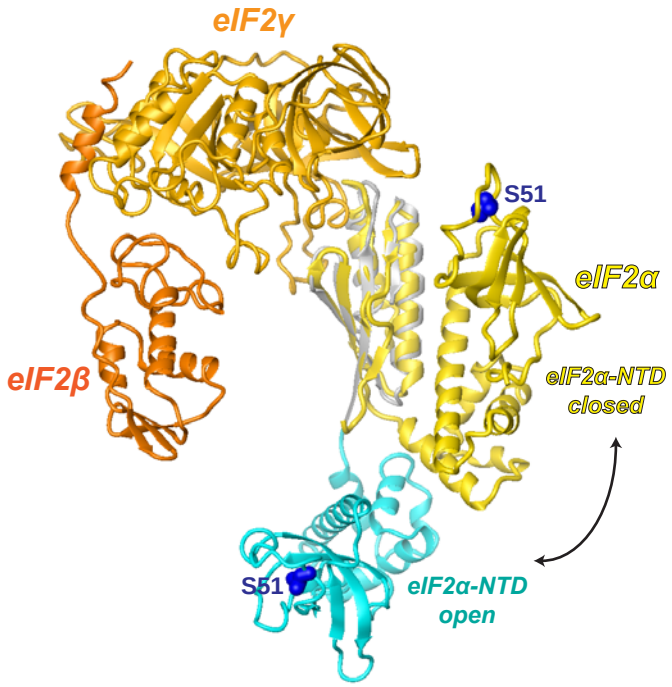

B **Effect of the S51D mutation on eIF2α mobility in GFC**

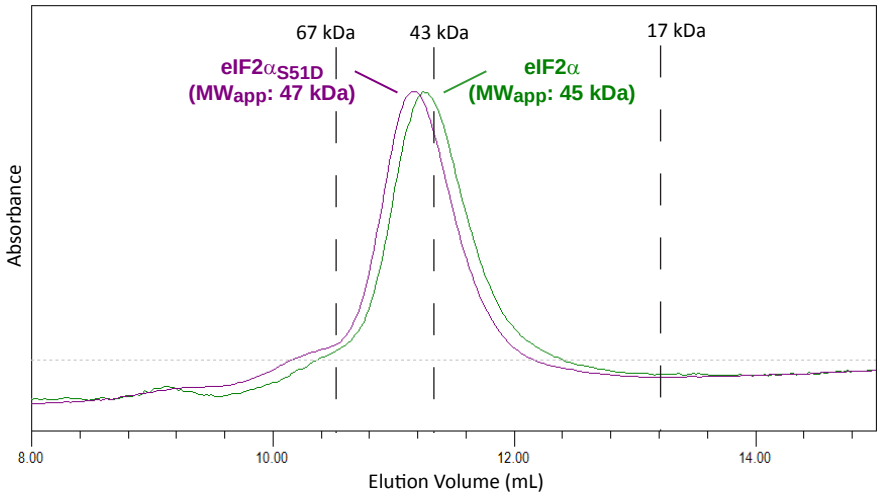

Figure S3.

(A) ***Closed eIF2α conformation in the context of the eIF2 structure.*** aIF2 from the structure of the archaeal eIF2-GTP•Met-tRNA$_i$ complex (3V11.pdb) (2) is shown as ribbon. aIF2β is orange-red; aIF2γ is orange; aIF2α-CTD is grey; and aIF2α-NTD is grey. The CTD of human eIF2α (shown in yellow) in closed conformation, as in **Fig. 1E**, was aligned to the CTD of aIF2α. The side-chain of S51 is shown in blue. eIF2α is in orientation similar to that in **Fig. 1E**.

(B) ***Effects of the phosphomimetic S51D mutation on eIF2α mobility in Gel Filtration Chromatography (GFC).*** GFC traces of WT eIF2α (green) and eIF2α$_{S51D}$ (magenta). The proteins were run on a GE Superdex G 75 10/300 GL column, in a 10 mM Na phosphate buffer, pH 7.0, 150 mM NaCl, 0.01 % NaN3, 2 mM DTT, 0.1 mM AEBSF, 1 mM EDTA. Positions of select molecular weight markers are shown with dashed lines. MW$_{app.}$ was calculated from a standard curve using molecular weight markers.

Fig. S4

A eIF2Bα Binding Surface on eIF2α-NTD

B eIF2Bα Binding Surface on eIF2α

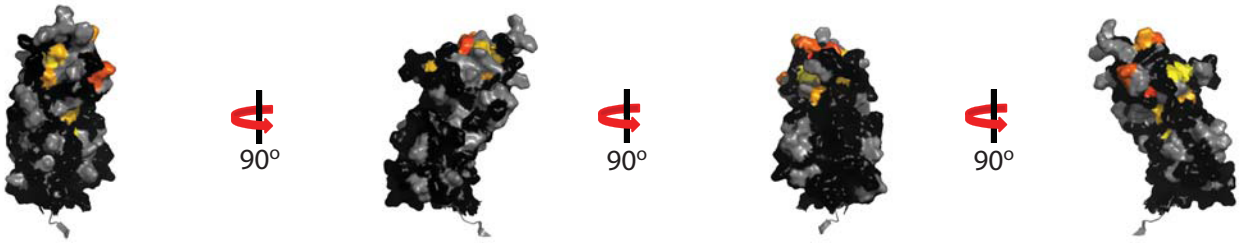

C eIF2Bα Binding Surface on eIF2α-NTD$_{S51D}$

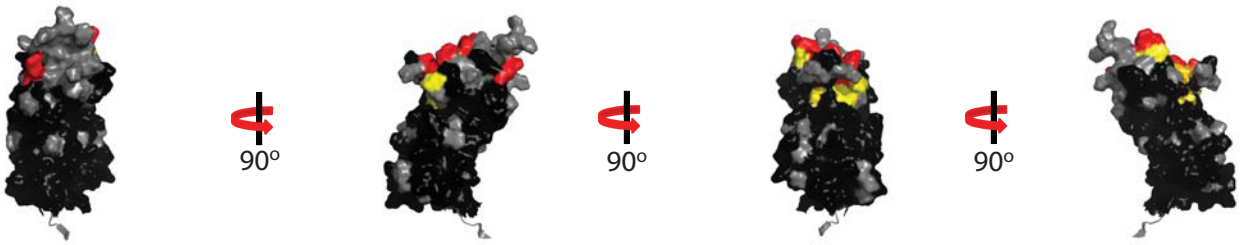

D eIF2Bα Binding Surface on eIF2α$_{S51D}$

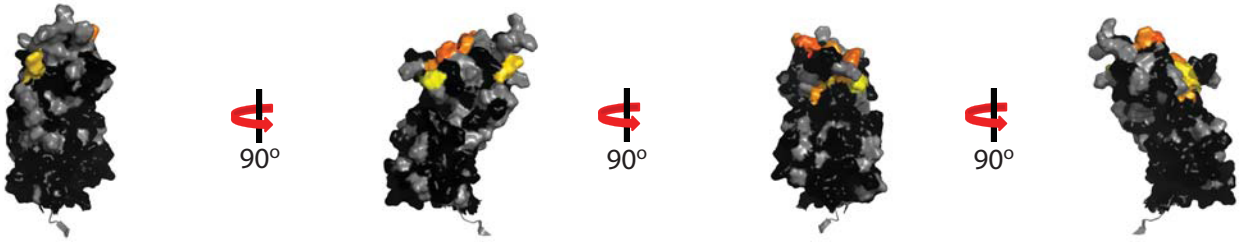

Figure S4. Effects of the phosphomimetic S51D mutation and eIF2α-CTD on eIF2Bα binding

Residues in eIF2α-NTD **(A)**, eIF2α **(B)**, eIF2α-NTD$_{S51D}$ **(C)**, and eIF2α$_{S51D}$ **(D)** experiencing selective signal loss in TROSY-HSQC spectra of $^{2}H/^{15}N$-labeled protein samples upon binding to eIF2Bα, mapped onto the structure of eIF2α-NTD, colored from **yellow** (>1σ) to **red** (>3σ). Indeterminate residues are colored **grey**. Residues <1σ are colored **black**. eIF2α-NTD is shown in the same orientation as in **Fig. 3D**. For full length eIF2α and eIF2α$_{S51D}$, only the NTD is shown, as no residues in the CTD crossed the 1σ threshold. Surfaces appear similar for all four constructs, indicating no obvious change in binding to eIF2Bα due to the presence of eIF2α-CTD or due to the phosphomimetic mutation.

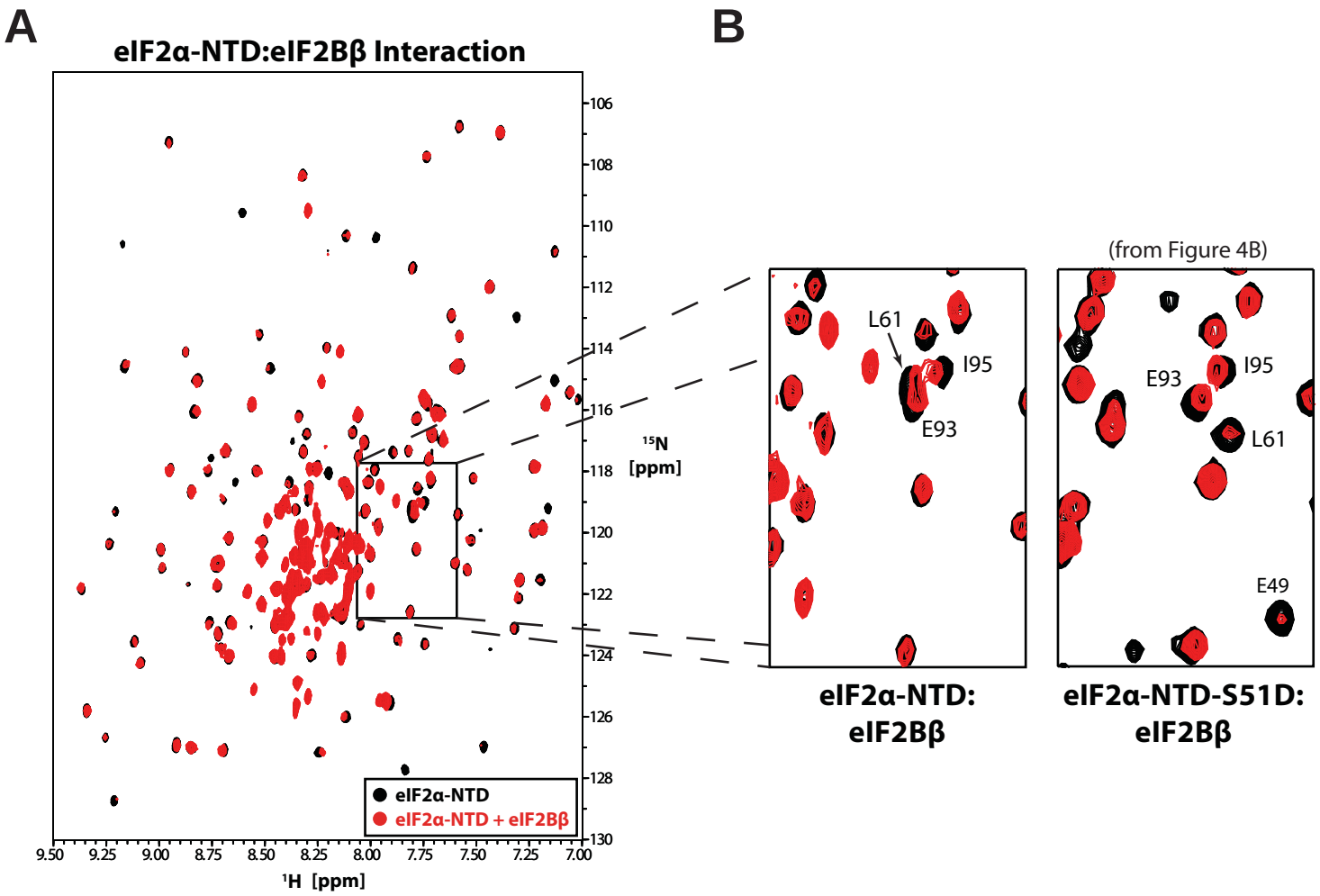
A
eIF2α-NTD:eIF2Bβ Interaction
eIF2α-NTD
eIF2α-NTD + eIF2Bβ
^{15}N [ppm]
^{1}H [ppm]
B
(from Figure 4B)
L61
I95
E93
E49
eIF2α-NTD: eIF2Bβ
eIF2α-NTD-S51D: eIF2Bβ

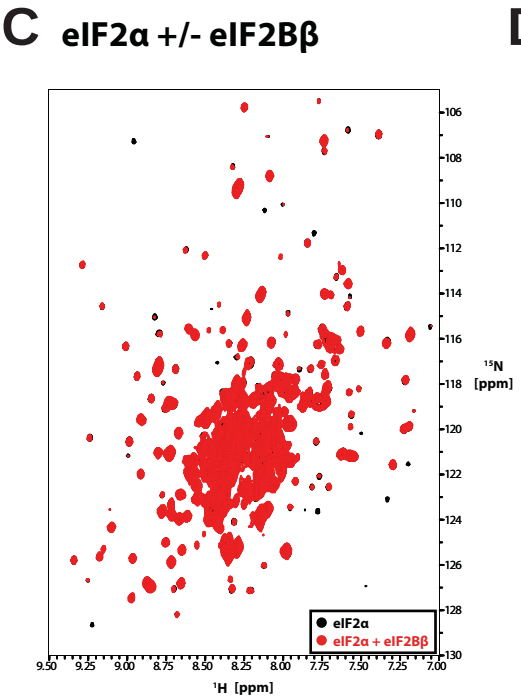
C eIF2α +/- eIF2Bβ
eIF2α
eIF2α + eIF2Bβ
^{15}N [ppm]
^{1}H [ppm]

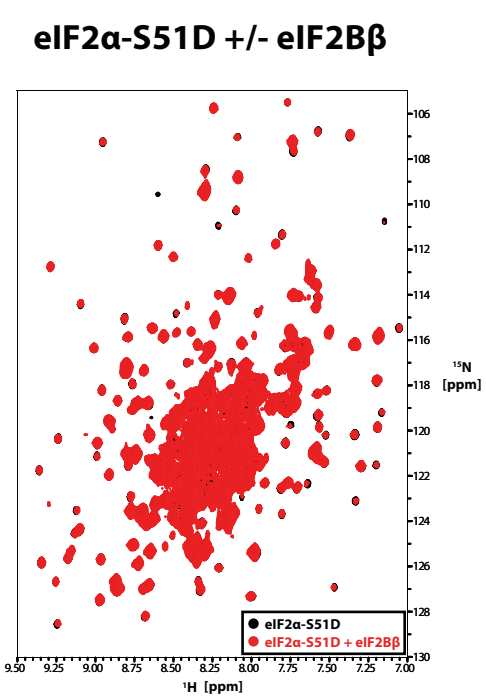
D eIF2α-S51D +/- eIF2Bβ
eIF2α-S51D
eIF2α-S51D + eIF2Bβ
^{15}N [ppm]
^{1}H [ppm]

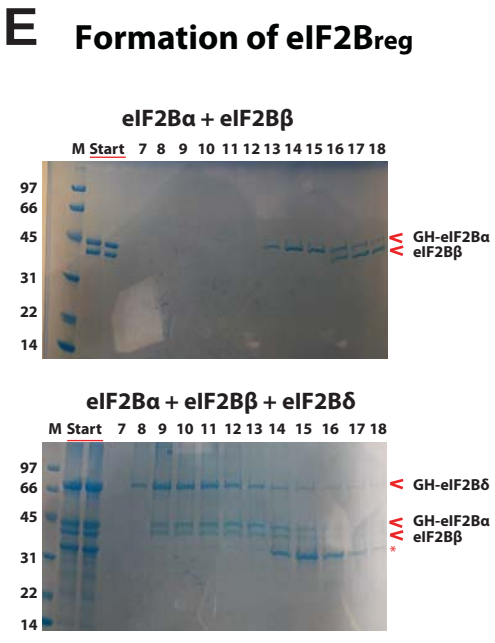
E Formation of eIF2Breg
eIF2Bα + eIF2Bβ
M Start 7 8 9 10 11 12 13 14 15 16 17 18
97
66
45
31
22
14
GH-eIF2Bα
eIF2Bβ
eIF2Bα + eIF2Bβ + eIF2Bδ
M Start 7 8 9 10 11 12 13 14 15 16 17 18
GH-eIF2Bδ
GH-eIF2Bα
eIF2Bβ

Figure S5. Effects of the phosphomimetic mutation S51D and eIF2α-CTD on eIF2Bβ binding

(A) TROSY-HSQC spectra of $^{2}H/^{15}N$-labeled eIF2α-NTD in the absence (**black**) and presence (**red**) of excess eIF2Bβ. **(B)** Boxed area in *(A)* with boxed area from **Fig. 4B** for comparison. Intermolecular surface was similar to that of eIF2α-NTD_{S51D} shown in **Fig. 4D**. TROSY-HSQC spectra of $^{2}H/^{15}N$-labeled eIF2α **(C)** and $eIF2\alpha_{S51D}$ **(D)** in the absence (**black**) and presence (**red**) of excess eIF2Bβ. No significant binding was observed. **(E)** SDS PAGE of fractions from Gel Filtration Chromatography (GFC) of a mix of GH-eIF2Bα and eIF2Bβ (top), and GH-eIF2Bα, eIF2Bβ, and GH-eIF2Bδ (bottom). Free eIF2Bα is a dimer, whereas eIF2Bβ and eIF2Bδ are monomers. *M*, molecular weight markers, *Start,* starting material, *7-18*, GFC fraction numbers. The protein positions are labeled on the right. A truncated eIF2Bδ fragment is labeled with an asterisk (*).

A

Proposed eIF2 binding surface on eIF2B

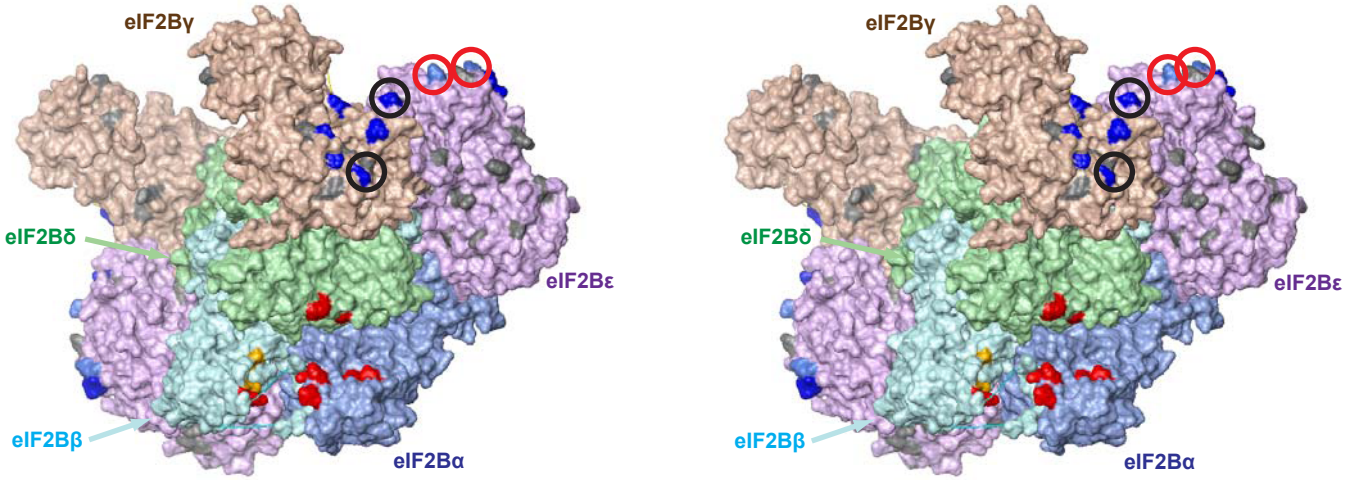

B

Docking the eIF2 ternary complex (TC) on the eIF2B structure

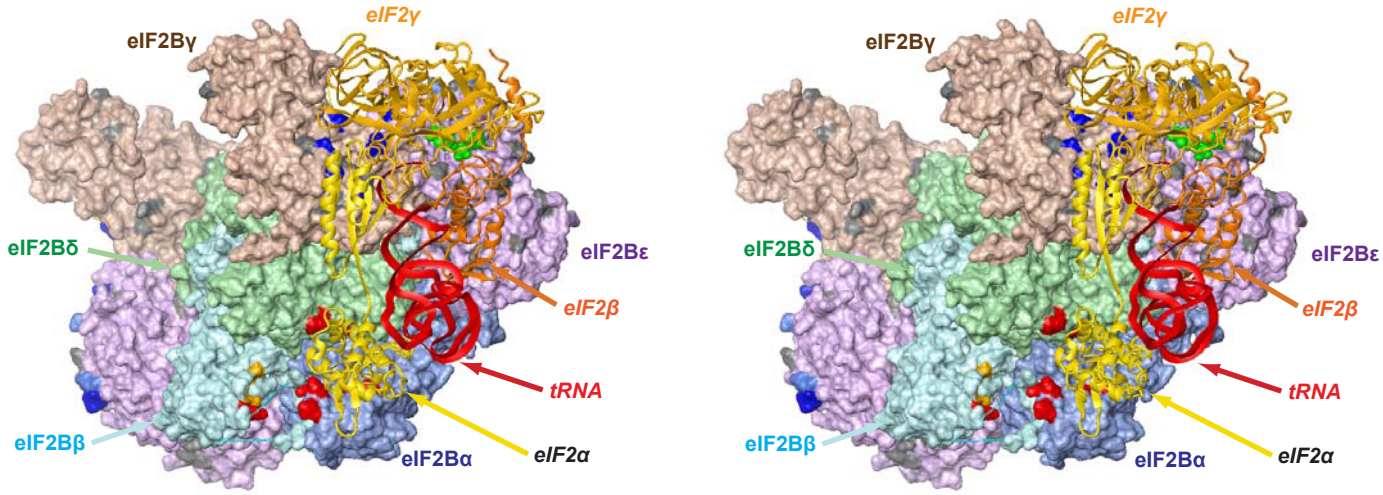

Figure S6. Docking the eIF2-TC on eIF2B

(A) Cross-eyed stereo view of the surface on eIF2B proposed to bind the eIF2 heterotrimer. eIF2Bα/β/δ residues shown to cross-link to both phosphorylated and unphosphorylated eIF2α are **red**; residues in eIF2Bβ that cross-link only to unphosphorylated eIF2α are **orange** (1). eIF2Bγ/ε residues shown to cross-link to eIF2γ in eIF2B•apo-eIF2 complexes are **navy**, except the two eIF2Bε residues with lower efficiency of cross-linking to eIF2(α-P)-GDP than to apo-eIF2 (1), which are **light blue**. The sites of CACH/VWM mutations in eIF2Bγε are **grey**. The same coloring scheme for eIF2B is used in panel *(B)* and in Figures S5B, S6, and S7. The two eIF2Bγ/ε residues shown to cross-link equally well to both apo-eIF2 and eIF2(α-P)-GDP (1) are marked with black circles. The two eIF2Bε residues with lower efficiency of cross-linking to eIF2(α-P)-GDP than to apo-eIF2 (1) are **light blue** and marked with red circles. **(B)** Cross-eyed stereo view of the eIF2-GTP•Met-tRNA$_i$ ternary complex (TC) from the *S. cerevisiae* 48S pre-initiation complex (3JAQ.pdb) (3) docked on eIF2B. eIF2B coloring is as in panel *(A)*. eIF2-TC is shown as ribbon.

A **Model of the eIF2B:TC complex with eIF2B colored by electrostatic potential**

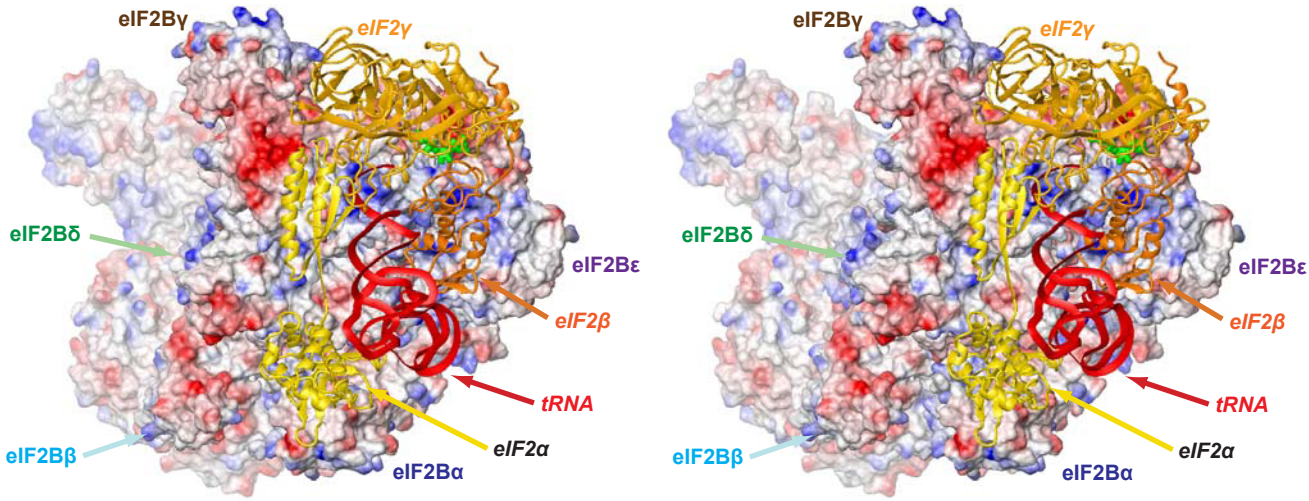

B **Model of the eIF2B:TC complex with positions of cross-links**
(GTP and Met-tRNA$_i$ are not shown)

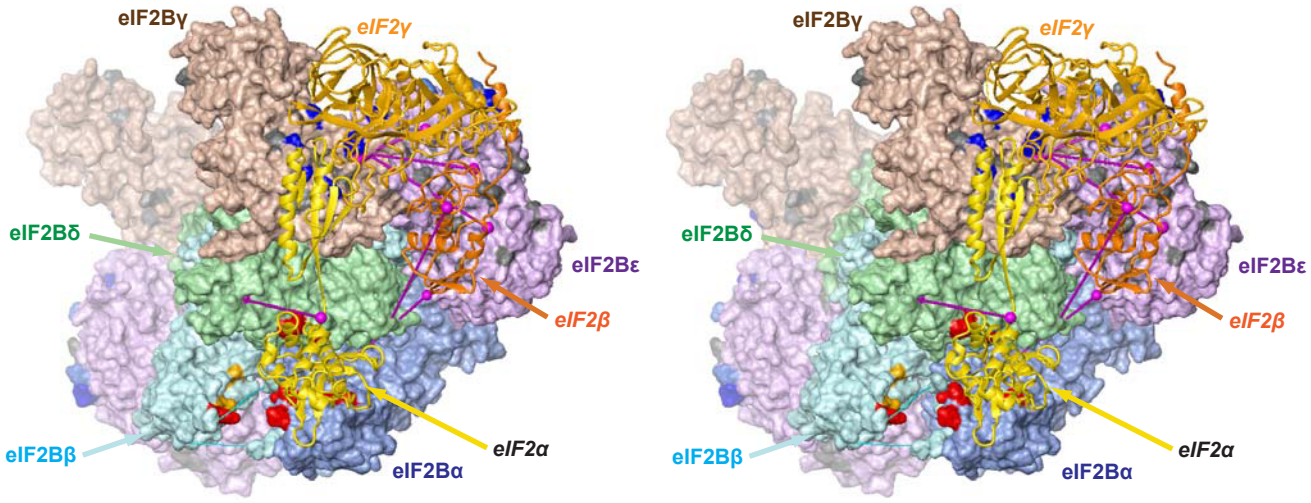

Figure S7. Validating the eIF2B•TC model

(A) Cross-eyed stereo view of the eIF2B•TC complex, with eIF2B colored based on electrostatic potential (blue indicates positive charges; red indicates negative charges). The color scheme of TC is as in **Fig. S6B**. **(B)** Cross-eyed stereo view of the eIF2B•TC complex, with eIF2B and eIF2 residues reported to cross-link to each other (4) shown in **magenta** and connected with **magenta** lines). The tRNA and nucleotide are not shown so as not to visually obscure cross-links. eIF2B and eIF2 coloring is as in **Fig. S6B**.

A

Docking eIF2Bε-CTD on the eIF2B:TC complex

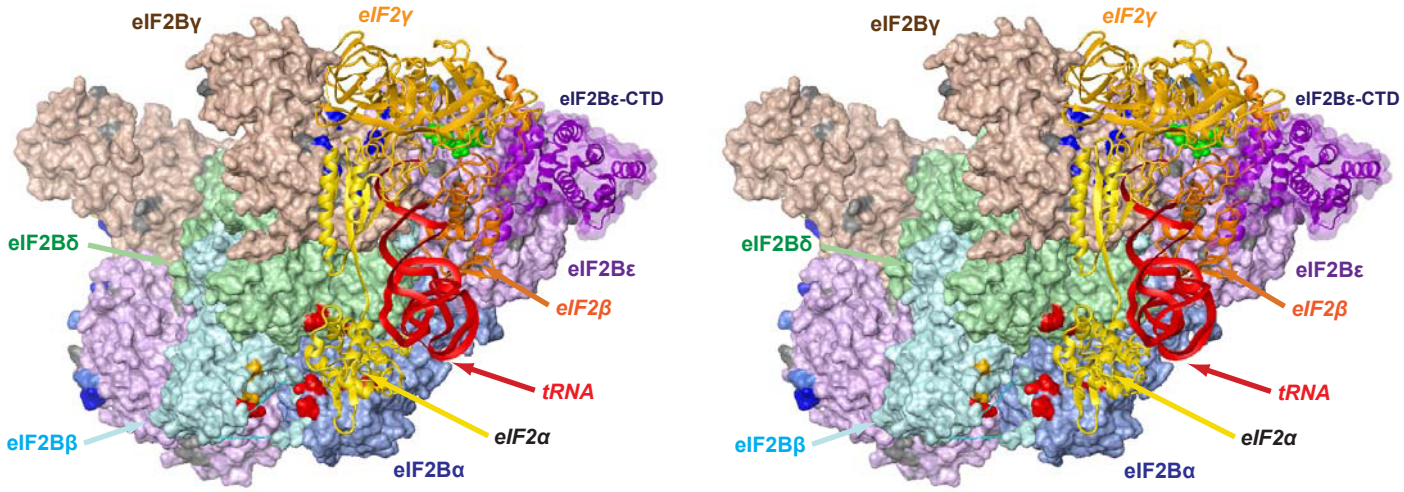

B

Merging the eIF2B:eIF2 model and eIF2B:TC model

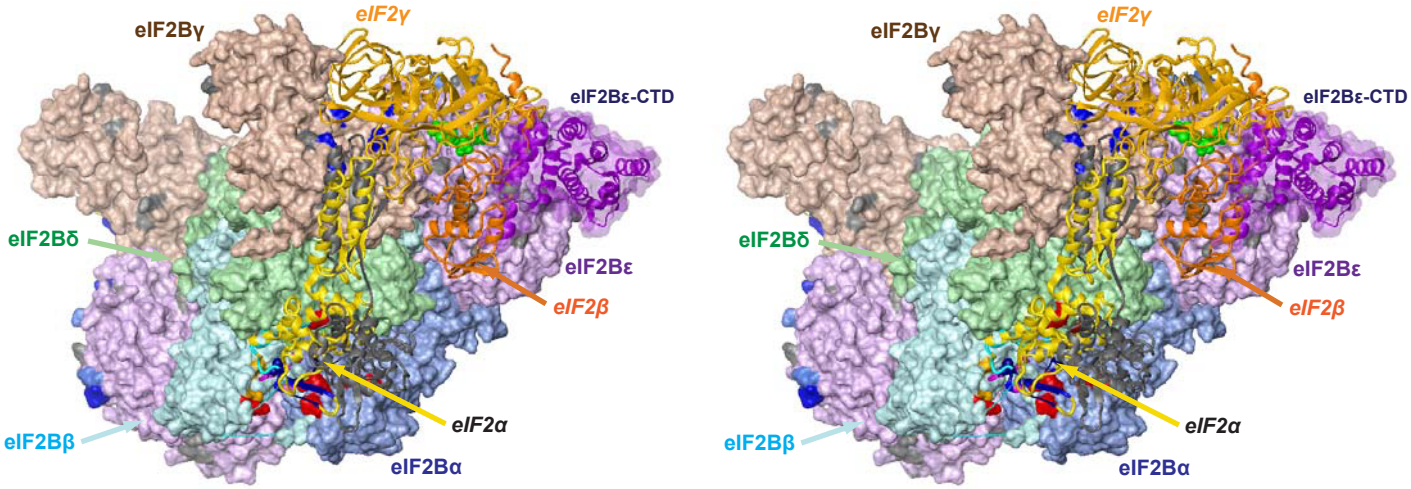

Figure S8. Building a model of the eIF2B•eIF2(α-P)-GDP complex

(A) Cross-eyed stereo view of the eIF2B•TC with the structure of human eIF2Bε-CTD (3JUI.pdb) (5) docked such that it interacts with a CACH/VWM mutation-rich surface on eIF2Bε as well as oriented such that residues important for catalytic activity are facing the G-domain of eIF2γ. eIF2B and eIF2 coloring is as in **Fig. S6B**. **(B)** Cross-eyed stereo view of the eIF2B•eIF2α model shown in **Fig. 6A** merged with the model of the eIF2B•TC complex shown in **Fig. 6B**. eIF2α from the eIF2B•eIF2α model is colored **yellow**, with individual residues in eIF2α colored according to the following scheme: (i) residues in the P-loop are **purple**, unless colored as detailed below; (ii) residues affected by eIF2Bα binding (see **Fig. 3**) are **navy**; (iii) residues affected by eIF2Bβ binding (see **Fig. 4**) are **cyan**; and (iv) residues affected by both are **blue**. eIF2α from the eIF2B•TC model is colored **grey**. The tRNA is not shown.

A

Potential ligand-binding sites in eIF2B

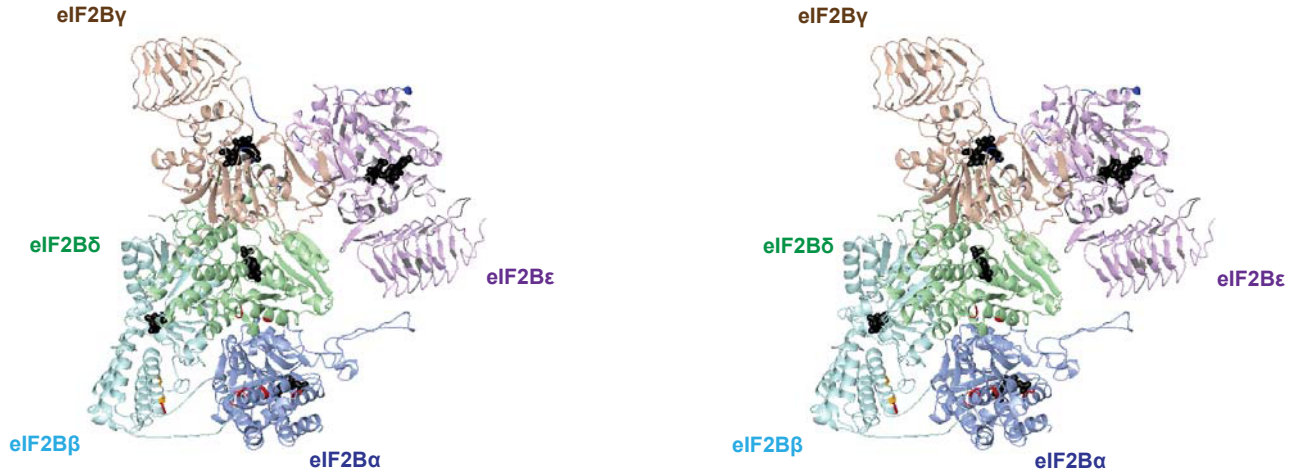

B

Positions of ligand-binding sites indicate possible effects on eIF2 binding/nucleotide exchange

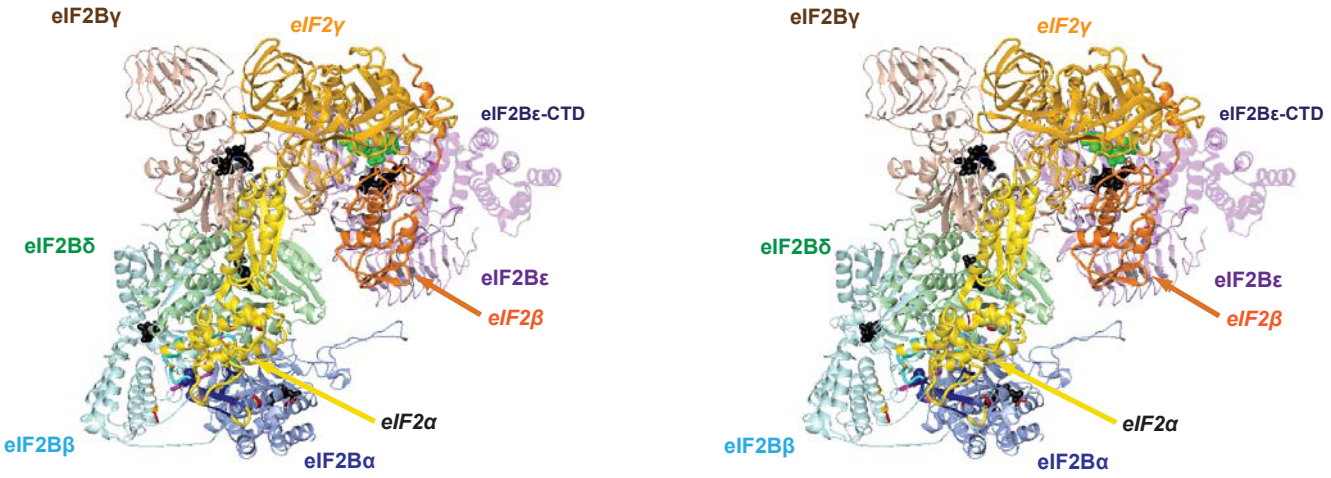

C

Model of the eIF2B:eIF2 complex
(shown for reference)

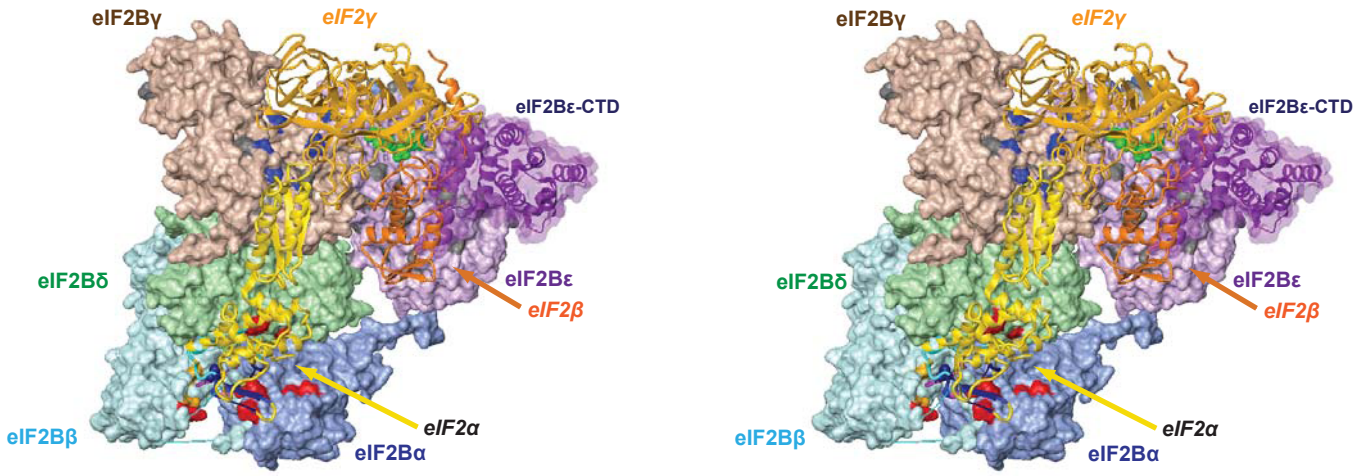

Figure S9. Potential mechanisms of eIF2B regulation by small molecules

(A) Cross-eyed stereo view of eIF2B in ribbon representation with potential ligand-binding locations shown as **black** spheres. Only one copy of each subunit is displayed for simplicity. eIF2B coloring is as in **Fig. S6**. **(B)** The same view as in *(A)*, but with eIF2(α-P)-GDP overlaid. eIF2B coloring is as in panel *(A)*. eIF2 coloring is as in **Fig. S8B**. **(C)** The same view as in *(B)*, but with eIF2B in surface representation.

Supplementary References

1. Kashiwagi, K., Takahashi, M., Nishimoto, M., Hiyama, T.B., Higo, T., Umehara, T., Sakamoto, K., Ito, T. and Yokoyama, S. (2016) Crystal structure of eukaryotic translation initiation factor 2B. *Nature*, **531**, 122-125.
2. Schmitt, E., Panvert, M., Lazennec-Schurdevin, C., Coureux, P.D., Perez, J., Thompson, A. and Mechulam, Y. (2012) Structure of the ternary initiation complex aIF2-GDPNP-methionylated initiator tRNA. *Nat Struct Mol Biol*, **19**, 450-454.
3. Llacer, J.L., Hussain, T., Marler, L., Aitken, C.E., Thakur, A., Lorsch, J.R., Hinnebusch, A.G. and Ramakrishnan, V. (2015) Conformational Differences between Open and Closed States of the Eukaryotic Translation Initiation Complex. *Mol Cell*, **59**, 399-412.
4. Gordiyenko, Y., Schmidt, C., Jennings, M.D., Matak-Vinkovic, D., Pavitt, G.D. and Robinson, C.V. (2014) eIF2B is a decameric guanine nucleotide exchange factor with a gamma2epsilon2 tetrameric core. *Nat Commun*, **5**, 3902.
5. Wei, J., Jia, M., Zhang, C., Wang, M., Gao, F., Xu, H. and Gong, W. (2010) Crystal structure of the C-terminal domain of the varepsilon subunit of human translation initiation factor eIF2B. *Protein Cell*, **1**, 595-603.